Construction of 2D/2D g-C3N4/CeO2 heterojunction and its oxygen vacancy mediated photocatalytic activity

Huihu Wang, Hao Tu, Haiping Hu, Yuan Chen, Pascal Boulet, Marie-Christine Record

Construction of 2D/2D g-C_3N_4/CeO_2 Heterojunction and its Oxygen Vacancy Mediated Photocatalytic Activity

Huihu Wang[a,b,c,*], Hao Tu[a,b,c], Haiping Hu[a,b,c], Yuan Chen[a,b,c*], Pascal Boulet [d,e], Marie-Christine Record [d,e]

a Hubei Provincial Key Laboratory of Green Materials for Light Industry, Hubei University of Technology, Wuhan, P. R. China

b Hubei Longzhong Laboratory, Xiangyang 441000, Hubei, China

c New Materials and Green Manufacturing Talent Introduction and Innovation Demonstration Base, Hubei University of Technology, Wuhan 430068, Hubei, China

d Aix-Marseille Univ., IM2NP, 13397 Marseille Cedex 20, France

e CNRS, IM2NP, 13397 Marseille Cedex 20, France

Corresponding authors:

Huihu Wang; Yuan Chen

E-Mail Address: wanghuihu@hbut.edu.cn; chen.yuan@hbut.edu.cn

Tel. +86-27-59750460

Fax. +86-27-59750460

Abstract

CeO_2 sheets (CeO_2-S) through hydrogen treatment (CeO_2-S-H_2) have been coupled with carboxylated g-C_3N_4 (C-g-C_3N_4) to construct 2D/2D C-g-C_3N_4/CeO_2-S-H_2 heterojunction. The ratio of Ce^{3+}/Ce^{4+} in CeO_2-S was increased from 28.2% to 32.08% in CeO_2-S-H_2. Experiment results demonstrated the highest CO yields in 8 h of 60%C-g-C_3N_4/CeO_2-S-H_2 were 2.41, 6.83 and 1.72 times of that of pure C-g-C_3N_4, CeO_2-S and CeO_2-S-H_2. Heterojunction also exhibited the highest CH_4 yields of 11.997 μmol/g in 8 h. Interestingly, CH_4 yield of CeO_2-S-H_2 was much higher than that of CeO_2-S, verifying oxygen vacancy introduction can effectively enhance CH_4 production. In addition, 60%C-g-C_3N_4/CeO_2-S-H_2 heterojunction demonstrated the best ciprofloxacin degradation performance. It is suggested that the synergistic effects of oxygen vacancy introduction and heterojunction construction promoted charges transfer and separation.

Keywords

Semiconductors; Nanocomposites; g-C_3N_4; CeO_2; Oxygen vacancy

1. Introduction

In rencent years, the construction of g-C_3N_4/CeO_2 heterojunction with high redox capability has attracted extensive attention because of their good band matching and the reverse redox characteristics [1-3]. Among different heterostructures, 2D/2D structure has significant advantages of the enhanced light absorption, large contact area and rich active sites [4]. However, photocatalytic performance of 2D/2D g-C_3N_4/CeO_2 heterojunction still faces great limitations mainly due to large size of 2D CeO_2. The modified strategies are quite needed.

It is known that defects inevitably exist for single semiconductor material, which may cause the rearrangement of charges around them and form the localized electronic states in space and corresponding defect state energy level. When surface defects energy levels meet the thermodynamic conditions of catalytic reaction, surface defects have the advantages of providing active sites and improving charges transfer. Thus, it is expected that photocatalytic activity of 2D/2D g-C_3N_4/CeO_2 structure can be significantly improved by introducing defects into CeO_2. Herein, we report the oxygen vacancy mediated method to construct g-C_3N_4/CeO_2 heterostructure through hydrogen treatment on CeO_2. CO_2 reduction and organic pollutants degradation performance were investigated. The inherent catalytic mechanism of heterojunction was also discussed.

2 Experimental

2.1 Synthesis of Photocatalysts

For CeO_2-S preparation, 0.75 mmol of $Ce(NO_3)_3 \cdot 6H_2O$, 0.6 mL of acetic acid and 5.25 mmol of hexamethylenetetramine were firstly dissolved in 15 mL of deionized water. Then, the solutions were hydrothermally treated at 140 °C for 9 h to obtain precipitates, which were further annealed in muffle furnace at 500 °C for 2 h. As-obtained CeO_2-S was light yellow. To regulate surface oxygen vacancy, CeO_2-S was further treated in gas mixtures of hydrogen (5%) and argon (95%) at 500 °C for 2 h. The colour of CeO_2-S-H_2 was gray white.

C-g-C_3N_4 was synthesized by refluxing g-C_3N_4 bulks in HNO_3 solution [5]. For C-g-C_3N_4/CeO_2-S-H_2 preparation, a certain amount of C-g-C_3N_4 and CeO_2-S-H_2 with total mass of 0.5 g were firstly mixed. C-g-C_3N_4 content was accounted for 20%, 40%, 60% and 80% respectively. Secondly, solid mixtures were dispersed in 50 mL of methanol solution by ultrasonication and magnetic stirring. Finally, solid powderz were calcined at 150 °C for 4 h. Specific preparation process is shown in Scheme S1. Characterization techniques and photoelectrochemical measurement were shown in supplementary materials.

2.2 Photocatalytic Test

CO_2 reduction was carried out in a 120 mL of cylindrical glassware reactor, in which 50 mg of catalyst powders was firstly placed inside. Before reaction, high purity CO_2 (99.99%) gas flushed the reactor. 2 mL of deionized water was injected into the reactor as reducing agent. A 300 W Xe lamp ($\lambda >$ 400 nm) was used as light source. Target products were analysed using gas chromatography with FID detector. For ciprofloxacin (CIP) degradation, 50 mg of catalyst was dispersed in 100 mL of CIP aqueous solution (10 mg/L). Typically, suspensions were magnetically stirred in dark for 30 min. Afterwards, it was irradiated by 300 W Xe lamp ($\lambda >$ 400 nm). CIP concentration was analysed by UV-visible spectrophotometer (Shimadzu UV-2600, Japan).

3 Results and Discussion

Fig.1 shows the morphologies of photocatalysts. Typical diffraction peaks of both g-C_3N_4 and CeO_2 phases have been observed in patterns of C-g-C_3N_4/CeO_2-S-H_2 (Fig.S1). C-g-C_3N_4 morphology mainly presents nanosheets and nanoparticles (Fig.1a), while CeO_2-S is composed of sheets with diameter of about 200-500 nm (Fig.1b). A layer-to-layer stack-like sandwich structure is observed for 60%C-g-C_3N_4/CeO_2-S-H_2 (Fig.1c). It should be noted that hydrogen treatment has little effect on CeO_2-S morphology. TEM image of 60%C-g-C_3N_4/CeO_2-S-H_2 shows that CeO_2-S-H_2 sheets are evenly

distributed on C-g-C_3N_4 surface, and a 2D/2D stacked layered structure is formed (Fig.1d). High-resolution TEM image displays (Fig.1e) the lattice spacing of CeO_2-S-H_2 is 0.19 nm, which corresponds to (110) crystal plane. These results demonstrate C-g-C_3N_4/CeO_2-S-H_2 was successfully prepared. Elements mapping of 60%C-g-C_3N_4/CeO_2-S-H_2 (Fig.1f-Fig.1j) displays C, N, Ce, and O elements are uniformly distributed, which further ensures that a 2D/2D structure is constructed.

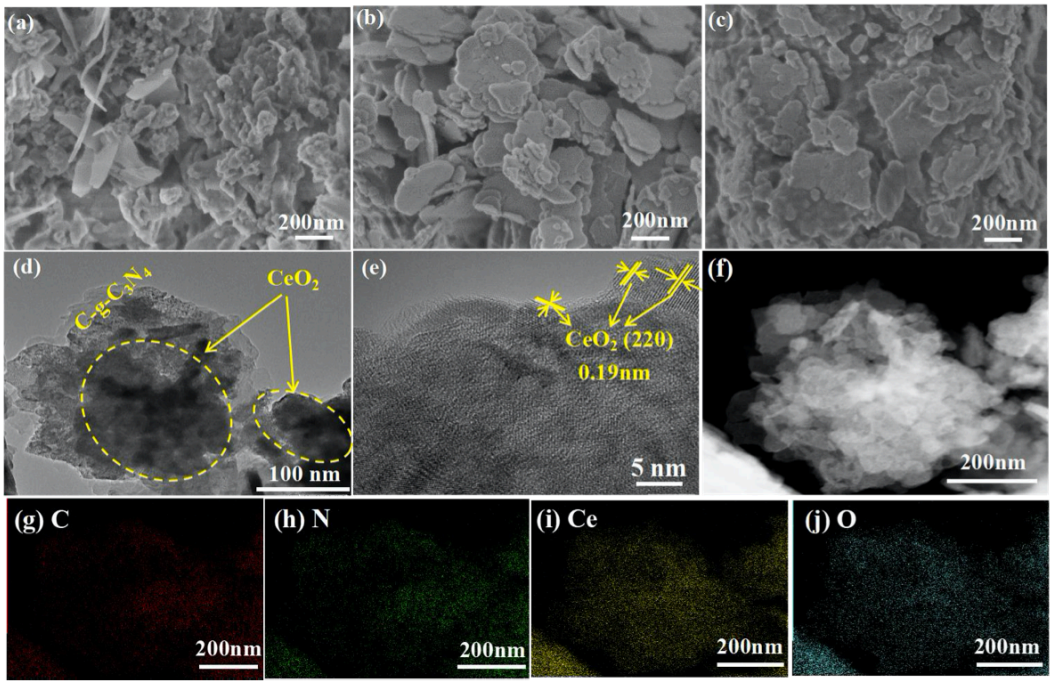

Fig.1 SEM images of C-g-C_3N_4 (a), CeO_2-S (b), and 60%C-g-C_3N_4/CeO_2-S-H_2 (c). TEM images (d, e) and element mapping images of 60%C-g-C_3N_4/CeO_2-S-H_2 (f, g, h, i, j)

To verify the effects of hydrogen treatment on surface defects, XPS spectra, TG analysis and Raman spectra were performed. As indicated in Fig.2a, C, N, O and Ce elements have been observed in the survey scanning spectra. Fig.2b shows high-resolution Ce 3d spectra. Ce 3d orbitals of CeO_2-S can be fitted into 8 peaks. Binding energies centered at 883.93 eV and 902.28 eV are due to Ce^{3+} states, and the other binding energy peaks are characteristics of Ce^{4+} states in CeO_2 [6]. The ratio of Ce^{3+} to Ce^{4+} in CeO_2-S is 28.2%, while it is 32.08% in CeO_2-S-H_2, which shows that oxygen vacancy content increases after hydrogen treatment. For CeO_2-S-H_2 and 60%C-g-C_3N_4/CeO_2-S-H_2, the position of Ce 3d peak has slightly changed due to the varied chemical environment. The other high-resolution XPS spectra of C1s, N1s and O1s can be found in Fig.S2. In Fig.2c, pristine C-g-C_3N_4 sample has mass loss at about 340 °C due to carboxyl groups decomposition, which is consistent with FTIR results in Fig.S3. Mass loss of CeO_2-S is relatively higher than that of CeO_2-S-H_2 due to oxygen escaping from lattice at

high temperature. Compared with pure C-g-C_3N_4, the introduction of CeO_2-S-H_2 has resulted in decomposition temperature decrease for C-g-C_3N_4/CeO_2-S-H_2 heterojunction. Fig.2d shows Raman spectra of CeO_2-S and CeO_2-S-H_2. The sharp characteristic peak at 460 cm^{-1} corresponds to F2g vibration mode (Ce-O), while the weak peak at 600 cm^{-1} is caused by oxygen vacancy [7].The peak intensity of CeO_2-S-H_2 at 600 cm^{-1} is higher than that of CeO_2-S, which further proves that hydrogen treatment has led to the increase of oxygen vacancy in CeO_2 lattice.

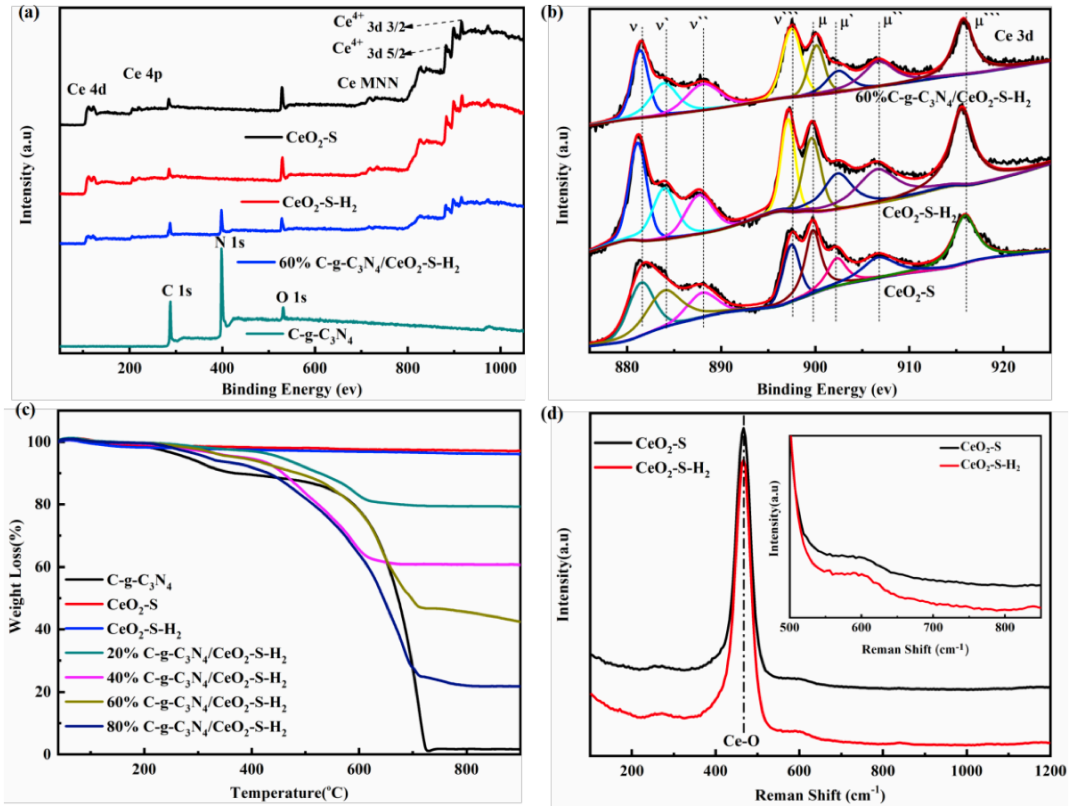

Fig.2 Survey scanning spectra (a) and high-resolution Ce 3d spectra (b) of CeO_2-S, CeO_2-S-H_2, and 60%C-g-C_3N_4/CeO_2-S-H_2. TG curves of C-g-C_3N_4, CeO_2-S, CeO_2-S-H_2 and C-g-C_3N_4/CeO_2-S-H_2 heterojunctions (c) and Raman spectra of CeO_2-S and CeO_2-S-H_2 samples (d)

Fig.3a shows CIP degradation curves. CIP degradation efficiency of 60%C-g-C_3N_4/CeO_2-S-H_2 reaches 78.5% within 120 min, which are 3 times, 7.48 times and 2.34 times of that of pristine C-g-C_3N_4 (26.1%), CeO_2-S (10.5%) and CeO_2-S-H_2 (33.5%). Degradation rate constant of 60%C-g-C_3N_4/CeO_2-S-H_2 is 5.027, 15.347 and 3.916 times of that of C-g-C_3N_4, CeO_2-S and CeO_2-S-H_2 (Fig.3b). Fig.3c and 3d show CO and CH_4 yields on different photocatalysts. CO yields on C-g-C_3N_4, CeO_2-S, CeO_2-S-H_2 and 60%C-g-C_3N_4/CeO_2-S-H_2 are 7.904 μmol/g, 2.785 μmol/g, 11.040 μmol/g and 19.032 μmol/g, while CH_4 yields are 0.261 μmol/g, 5.139 μmol/g, 11.211 μmol/g and

11.997 μmol/g. Especially, CO_2 reduction on CeO_2-S-H_2 is much better than CeO_2-S, which may be related to the increase of oxygen vacancy content. Interestingly, CH_4 yields on C-g-C_3N_4 is negligible. However, 60%C-g-C_3N_4/CeO_2-S-H_2 exhibits the highest CH_4 yields in 8 h, demonstrating heterojunction has advantages of both single components.

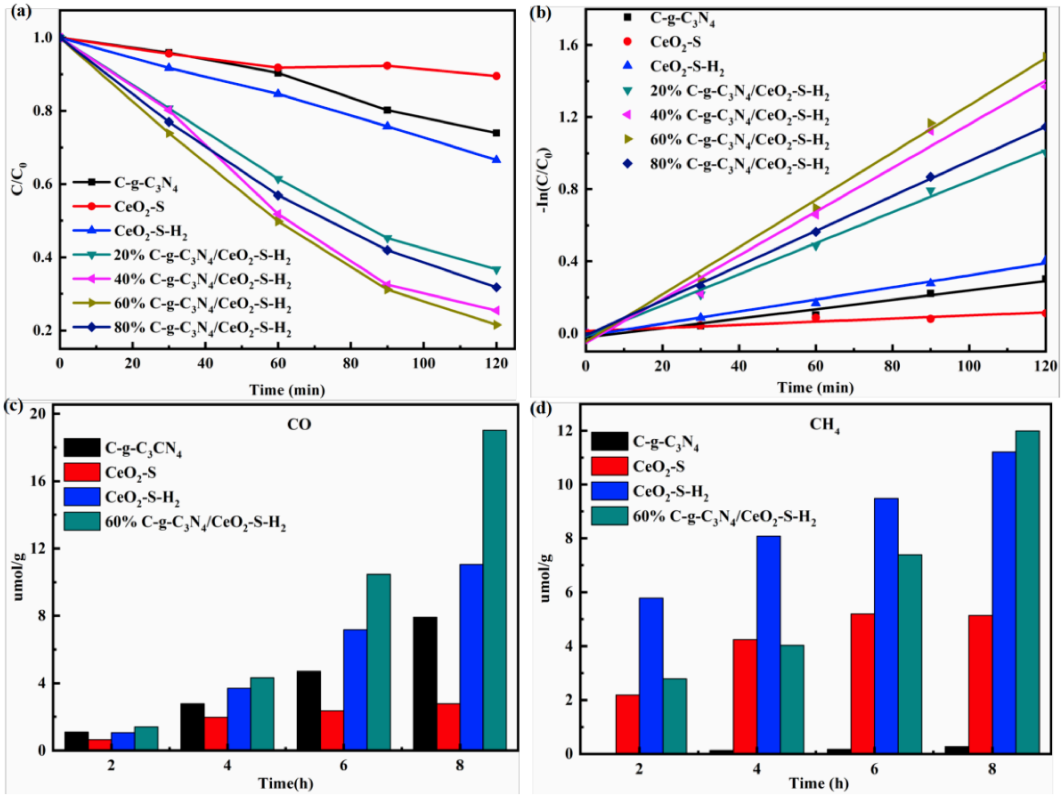

Fig.3 CIP degradation curves (a), first-order reaction kinetics curves (b), CO yields (c) and CH_4 yields (d) using C-g-C_3N_4, CeO_2-S, CeO_2-S-H_2 and C-g-C_3N_4/CeO_2-S-H_2 samples

Charges transfer and separation is of significance for photocatalytic activity enhancement. In Fig.4a, 60%C-g-C_3N_4/CeO_2-S-H_2 heterojunction displays the strongest photocurrent response. Accordingly, its semicircular diameter of Nyquist curve is the smallest as depicted in Fig.S4. Similarly, it shows the lowest photoluminescence intensity (Fig.4b). The corresponding transient PL was also depicted in Fig.S5. All these results demonstrate that heterojunction has enhanced charges separation efficiency. More charges will participate in the reaction. In Fig.4c, trapping experiments were carried out using 60%C-g-C_3N_4/CeO_2-S-H_2 as photocatalyst for CIP degradation. 1 mmol potassium iodide (KI), 1 mmol isopropanol (IPA) and nitrogen (N_2) were used as h^+, •OH and $•O_2^-$ scavengers. It can be observed that •OH is the most important active species involved in CIP degradation. h^+ is one of the major active species, which can seriously suppress heterojunction acivity. However, $•O_2^-$ is not a major

active species.

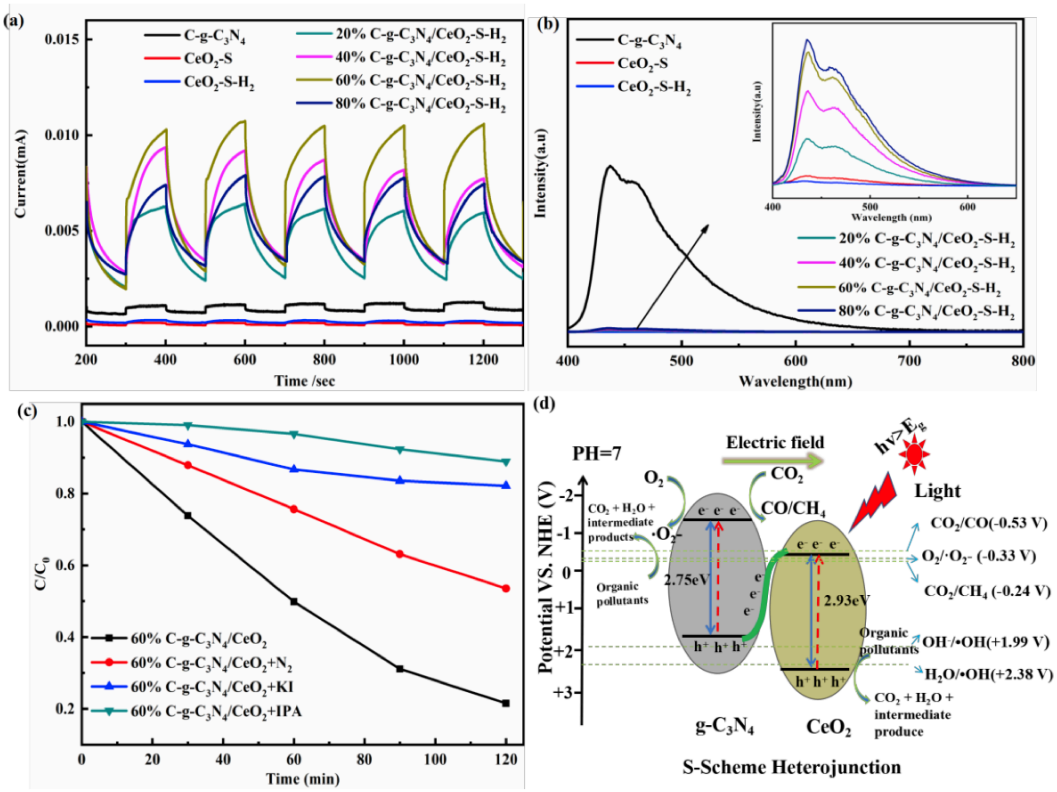

Fig.4 Transient photocurrent responses (a) and PL spectra of C-g-C_3N_4, CeO_2-S, CeO_2-S-H_2, C-g-C_3N_4/CeO_2-S-H_2 heterojunction.Trapping experiments of CIP degradation by 60%C-g-C_3N_4/CeO_2-S-H_2 heterojunction (c) and proposed photocatalytic mechanism

Band gaps of C-g-C_3N_4 and CeO_2-S-H_2 have been calculated as 2.75 eV and 2.93 eV from UV-Vis DRS spectra (shown in Fig.S6). According to the Mulliken's electronegativity theory formula [8], VB and CB positions of C-g-C_3N_4 and CeO_2-S-H_2 are +1.615 eV, –1.135 eV and +2.535 eV, –0.395 eV. As O_2/•O_2^- reduction potential is -0.33 V (NHE, pH=7), C-g-C_3N_4 is more favorable for •O_2^- radicals formation due to its more negative CB potential. On the other hand, VB potential of CeO_2-S-H_2 is more positive than H_2O/•OH (+2.38 V vs. NHE) and OH^-/•OH (+1.99 V vs. NHE). Therefore, the photogenerated h^+ can react with H_2O molecules or OH^- to produce •OH radicals. In contrast, C-g-C_3N_4 cannot generate •OH radicals under the same conditions. Thus, an S-scheme photocatalytic mechanism is proposed in Fig.4d [2, 9]. For CO_2 reduction, CB potential of C-g-C_3N_4 is more negative than the potential required for CO/CO_2 (–0.53 V) and CH_4/CO_2 (–0.24 V) conversions. Therefore, it is easy to reduce CO_2 to CO or CH_4. In CO_2 reduction process, H_2O is firstly oxidized to H^+ and O_2 by holes. Meanwhile, CO_2 molecules are reduced to CO and CH_4 with the aid of H^+ and electrons. It should be

noted that oxygen vacancy in CeO_2-S-H_2 can be used as electrons capture centers. As a result, electrons enrichment improves the kinetic conditions of CO_2 reduction, especially for CH_4 production. At the same time, oxygen vacancy can adsorb and activate CO_2 molecules, thus 2D/2D C-g-C_3N_4/CeO_2-S-H_2 heterojunction exhibits high CO and CH_4 yields in contrast to single components. In addition, Ce^{4+} in CeO_2-S-H_2 can enhance electrons capture to form Ce^{3+}, so as to promote charges separation and significantly improve photocatalytic activity.

4 Conclusions

In conclusion, C-g-C_3N_4 have been compounded with hydrogen treated flaky CeO_2-S-H_2 to construct 2D/2D C-g-C_3N_4/CeO_2-S-H_2 heterojunction. In contrast to pure components, 60%C-g-C_3N_4/CeO_2-S-H_2 exhibited the highest activity for CIP degradation and CO_2 reduction. Radicals trapping experiments showed •OH and h^+ were the two major active species in CIP degradation. The introduction of oxygen vacancy in CeO_2-S-H_2 has greatly enhanced CH_4 yields as it can be used as electron capture centers and promoted charges separation efficiency. Possible S-scheme mechanism of C-g-C_3N_4/CeO_2-S-H_2 was proposed.

Acknowledgements

This work was supported by the Wuhan Knowledge Innovation Project (2022010801010257) and the Independent Innovation Projects of the Hubei Longzhong Laboratory (2022ZZ-16).

References

[1] W. Q. Li, L. Jin, F. Gao, et al., Appl. Catal. B-Environ. 294 (2021) 120257. https://doi.org/10.1016/j.apcatb.2021.120257.

[2] S. Vignesh, S. Chandrasekaran, M. Srinivasan, et al., Chemosphere, 288(2022)132611, https://doi.org/ 10.1016/j.chemosphere.2021.132611.

[3] F. H. Xu, C. Lai, M. M. Zhang, et al., J. Colloid Interface Sci., 601(2021)196-208, https://doi.org/ 10.1016/j.jcis.2021.05.124.

[4] Y. Yuan, G.-F. Huang, W.-Y. Hu, et al., J. Phys. Chem. Solids. 106 (2017) 1-9. https://doi.org/10.1016/j.jpcs.2017.02.015.

[5] H. P. Hu, J. S. Hu, X. Y. Wang, et al., Catal. Sci. Technol. 10 (2020) 4712-4725. https://doi.org/10.1039/D0CY00395F.

[6] M. Li, L. Zhang, M. Wu, et al., Nano Energy. 19 (2016) 145-155. https://doi.org/10.1016/j.nanoen.2015.11.010.

[7] H. Wang, J. Guan, J. Li, et al., Appl. Surf. Sci. 506 (2020) 144931. https://doi.org/10.1016/j.apsusc.2019.144931.

[8] H. Xu, Y. Xu, H. Li, et al., Dalton Trans. 41 (2012) 3387-3394. https://doi.org/10.1039/C2DT11969B.

[9] P. Xia, S. Cao, B. Zhu, et al., Angew. Chem. Int. Ed. 59 (2020) 5218-5225. https://doi.org/10.1002/anie.201916012.